Entropy Changes in Water Networks Promote Protein Denaturation

Yichong Wang[1,2]†, Junlang Liu[1]†, Michael Peters[2], Ryoma Ishii[2,3], Dianzhuo Wang[1], Sourav Chowdhury[1,4], Kevin Kit Parker[2]*, Eugene I. Shakhnovich[1]*

Affiliations:

[1]Department of Chemistry and Chemical Biology, Harvard University; Cambridge, MA, 02138 USA.

[2]Disease Biophysics Group, John A. Paulson School of Engineering and Applied Sciences, Harvard University; Boston, MA, 02134 USA.

[3]Medical & Health Informatics Laboratories, NTT Research, Inc.; Sunnyvale, CA, 94085 USA.

[4]Medical Department of Biological Sciences, Birla Institute of Technology and Science-Pilani; Hyderabad, TN, 500078 India.

†These authors contributed equally to this work.

***Corresponding authors:**

Kevin Kit Parker
Science and Engineering Complex 6.307
150 Western Ave, Boston, MA 02134
Email: kkparker@seas.harvard.edu
Phone: 617-496-1793

Eugene I. Shakhnovich
12 Oxford Street
Cambridge, MA 02138
Email: shakhnovich@chemistry.harvard.edu
Phone: 617-495-4130

Abstract (121/125 words)

For over a century, an explanation for how concentrated ions denature proteins has proven elusive. Here, we report a novel mechanism of protein denaturation driven by entropy changes in water networks. Experiments and simulations show that ion pairs like LiBr and LiCl localize water molecules and disrupt the water network's structure, while others exert a more global effect without compromising network integrity. This disruption reduces the entropy penalty when proteins sequester water molecules during unfolding, resulting in a peculiar yet universal "inverse hydrophobic effect" that potentiates protein denaturation. Through successful isolation and systematic study of indirect solute effects, our findings offer a universal approach to salt induced protein denaturation and provide a unified framework for the decoding of the protein-water-solute nexus.

Introduction

In the 19th century, Franz Hofmeister discovered the 'Hofmeister Series' (*1*, *2*), describing how various salts can either increase or decrease protein solubility in aqueous solutions. Interest in this phenomenon grew between the 1940s and 1960s, focusing on how concentrated inorganic ions affect protein stability and conformation (*3*, *4*), with lithium bromide (LiBr) showing the most pronounced impact (*5–7*). While numerous studies observed distinct effects of various ions, the underlying mechanism of ion-induced denaturation lacked a comprehensive explanation due to limited experimental and theoretical approaches. In recent years, extensive research has explored the interactions between water molecules and ions (*8*, *9*), offering new insights into the origin of hydrophobicity and its influence on protein folding (*10–12*), potentially driven by modifications in the intermolecular interactions of water (*13*). However, a unified framework for understanding the triadic relationship between proteins, water, and solutes remains elusive (*14*).

Despite the use of ion-induced denaturation for extracting proteins such as keratin and silk fibroin (*15*, *16*), the gap between practical techniques and the lack of mechanistic insight limits our ability to fully control and utilize protein-based materials. The incomplete understanding of how ions contribute to this process has led to treating LiBr denaturants similarly to organic chemicals like urea or guanidine hydrochloride, which bind directly to proteins and require removal through dialysis (*17*). This complicates post-processing and restricts the implementation of widely adopted fabrication methods such as molding or fiber spinning (*18*). As a result, over ten million tons of keratin-rich waste are generated annually and typically disposed of through incineration or landfilling (*19*), regardless of their potential for applications ranging from textiles to tissue engineering scaffolds (*20*, *21*).

The phenomenon of protein denaturation is governed by the balance between opposing enthalpic and entropic driving forces. The gain in protein conformational entropy drives towards unfolding, as the polypeptide chain becomes more disordered. In contrast, enthalpic interactions between amino acids (e.g., Van der Waals forces, electrostatic interactions) and the increase in entropy of water molecules released from their interactions with non-polar side chains of proteins—known as the hydrophobic effect—stabilize the folded state under native conditions. Achieving denaturation requires overcoming the entropy penalty from the loss of potential water conformations as free water molecules are sequestered by proteins upon unfolding. One possible explanation for protein denaturation in concentrated ionic solutions is the indirect solute effect, which modulates the hydrophobic effect by altering the water hydrogen bond network (*13*).

To test this hypothesis, we selected a series of inorganic ion pairs—lithium bromide (LiBr), lithium chloride (LiCl), and sodium bromide (NaBr)—as model solutes, given their similar composition but distinct reported impacts on protein structures (*3*). We systematically explored the denaturation potency of these ionic solutes by evaluating their effects on three proteins spanning different levels of structural complexity, with LiBr emerging as the strongest universal denaturant and NaBr as the least potent. Both experimental and theoretical analyses revealed that these differences stem from the ion pairs' varying capabilities to modulate the water network rather than directly binding to the proteins. Through their local interactions with water molecules, ions like LiBr can significantly alter the structure of the water network, thereby reducing the entropy penalty associated with protein unfolding. Furthermore, this entropic denaturation mechanism offers significant advantages for extracting and regenerating keratin materials, enabling closed-loop recycling of the denaturant, simplifying the manufacturing process, and preserving the native shape-memory property.

87 **Universal denaturation capacity of LiBr**

88 To systematically investigate solute effects on protein conformation, we selected three proteins
89 representing different levels of structural complexity (Fig. 1A), along with three different ionic
90 solutes including LiBr, LiCl, and NaBr. We found markedly distinct solute effects for different
91 proteins and salts across various concentrations, as evidenced by aggregation of denatured protein
92 during turbidity measurements at 405 nm (Fig. 1, B to D). The smallest protein tested,
93 dihydrofolate reductase (DHFR) showed significant aggregation at 1 M LiBr and 5 M LiCl, but
94 remained soluble at all NaBr concentrations (Fig. 1B, and fig. S1). Since both salt-induced
95 precipitation and denaturation can result in protein aggregation, we used Fourier-transform
96 infrared spectroscopy (FTIR) to further distinguish the underlying mechanisms. Starting from 2 M
97 LiBr, we observed a gradual loss of secondary structure of DHFR such as α-helix (1650-1655 cm^{-}
98 ^{1}) and β-sheet/turns (1660-1690 cm^{-1}), along with an increase in aggregated β-like random
99 structures (1620-1630 cm^{-1}) (Fig. 1E). The secondary structure loss of DHFR in 2 M LiBr was
100 further confirmed by conformational kinetics measurement using quantitative Raman
101 spectroscopy, where less-stable β-sheet disappeared first, followed by α-helix, with obvious
102 accumulation of aggregated random structures (Fig. 1H, and figs. S2 and S3). Both FTIR and
103 tryptophan fluorescence measurement confirmed DHFR unfolding starting from ~5 M LiCl (fig.
104 S4, A and C). In contrast, DHFR stayed well-folded for all concentrations of NaBr.

105 To elucidate whether ionic solutes can affect conformations of proteins with more complex,
106 hierarchically ordered structures, we examined fibronectin. This protein, a critical component for
107 cell-extracellular matrix interactions (*22*) has more recently been explored as a synthetic building
108 material (*23–25*) because of its unique structure-function relationships. Fibronectin is comprised
109 of two covalently linked extensible arms formed by β-sheet domains that can undergo quaternary

110 structure changes from globular to extended state (*26*) (Fig. 1A middle). With the increase of
111 protein structural complexity, higher concentrations of LiBr and LiCl (7 M and 8 M, respectively)
112 were required to induce aggregation of fibronectin (Fig. 1C, and fig. S5), where secondary
113 structure loss was also confirmed by FTIR spectra (Fig. 1F, and fig. S4B). Before denaturation,
114 protein conformational changes were observed through dynamic light scattering (DLS)
115 measurements of the hydrodynamic radius R_h (Fig. 1I), where fibronectin transitions from the
116 globular state (R_h ~8 nm) to the extended state (R_h ~23 nm) at a lower concentration of LiBr around
117 2 M. Combining the loss of the secondary and tertiary structure observed in FTIR and the
118 quaternary structure extension shown via DLS, we can identify sequential changes in protein
119 structure as the concentration of LiBr increases (fig. S4D).

120 We also tested keratin structural transformation in LiBr solution as observed by
121 Feughelman et al. (*3*). In contrast to DHFR and fibronectin, keratin possesses hierarchical structure
122 ranging from α-helices at the nanometer scale to protofibrils and filaments at the micrometer scale.
123 A turbidity map generated from 24-hour soaking of wool in salt solutions showed that visible
124 signal can only be observed at high concentrations of LiBr (Fig. 1D). FTIR spectra further
125 indicated complete denaturation of both α-keratin from wool and β-keratin from goose feathers,
126 irrespective of their different native configurations (Fig. 1G). Finally, scanning electron
127 microscope (SEM) images of wool before and after treatment with 8 M LiBr, LiCl, and NaBr also
128 corroborate our turbidity measurement findings, where only concentrated LiBr induces
129 denaturation of keratin (Fig. 1J, fig. S4E, and fig. S6).

130 **Indirect solute effects**

131 Thermodynamically, protein conformational change or denaturation is a complex process where
132 entropy and enthalpy contribute to the overall free energy balance. At lower concentrations of

133 denaturants, entropy and enthalpy balance to favor the native state; however, at higher
134 concentrations, they tend towards the unfolded state (*27*). To elucidate the thermodynamic
135 mechanisms of protein denaturation by LiBr, we conducted isothermal titration calorimetry (ITC)
136 experiments to measure the enthalpic contribution from direct LiBr solute-protein interactions,
137 with commonly used denaturants urea and guanidine hydrochloride (GdnHCl) as a control.
138 Pronounced heat release was detected upon injection of urea or GdnHCl into samples containing
139 DHFR and fibronectin (Fig. 2, A and B, and fig. S7). Enthalpy changes, dependent on protein sizes
140 and exposures of hydrophobic domains (~-7 kCal mol^{-1} for DHFR and ~-14 kCal mol^{-1} for
141 fibronectin), correspond to the formation of 1-2 or 3-4 hydrogen bonds per organic denaturant
142 molecule, respectively. These results are consistent with previous studies (*28*, *29*), where enthalpy-
143 driven mechanisms of protein denaturation by urea or GdnHCl were established. In contrast, no
144 enthalpy change from direct interaction with proteins was detected when LiBr solution was
145 injected into protein samples under identical protocols, suggesting that solute ions here do not
146 engage in noticeable direct interactions with proteins. Given that LiBr, being a universal and potent
147 denaturant, does not contribute enthalpically to protein free energy in solution, we hypothesize
148 that LiBr shifts the free energy landscape of proteins towards denatured state by affecting its
149 entropy.

150 **Mechanism of entropy-driven protein denaturation**

151 To further test the hypothesis of entropy-driven denaturation by LiBr, molecular dynamics (MD)
152 simulations were employed to provide experimentally inaccessible atomistic-level insights. First,
153 we confirmed that local water density around ions (fig. S8, A and B) in our simulations agrees
154 well with previous X-ray and neutron diffraction experimental results (*30*). The cooperativity of
155 ion hydration (*31*) was also observed, where local water structures are determined by both ions

and their counterions. Molecular water entropy, encompassing both translational and rotational entropy of water molecules, was calculated based on TIP3P (*32*) water model using Two-Phase Thermodynamic (2PT) method, which has been validated as the most accurate for replicating experimental entropy values (*33*). In both LiBr and LiCl solutions, two distinct populations of water molecules are detectable (Fig. 2C). As suggested by evidence of local effects of Li^+ ions (*34*), the subset characterized by lower average entropy is identified as ion-bound water, whereas the other, possessing higher entropy, is identified as free water that constitutes the hydrogen bonded water network. LiBr solution also demonstrates a higher proportion of ion-bound water compared to LiCl solution (Fig. 2E, i, and fig. S8, C and D). This enhanced capacity of Li^+ ions to sequester water in LiBr could stem from the more effective separation between Li^+ and Br^- ions (*8*, *9*), attributable to the lower charge density of Br^- ions and the substantial size disparity between Li^+ and Br^- ions. In contrast, the NaBr solution exhibits a single population suggesting to the intact hydrogen bond network of pure water (Fig. 2E, ii, and fig. S8E), which could potentially be explained by the absence of localized high charge density (*9*, *31*).

The prominent differences in both water network size and denaturation capability between LiBr, LiCl, NaBr, and pure water, point out to fundamental change in water network entropy as a possible culprit. To further highlight this concept, we established an analytical model describing the decrease of total entropy penalty from water molecules in solution ($\Delta\Delta S^{\text{water}}$), which drives the overall free energy balance towards the denatured state.

$$\Delta\Delta S^{\text{water}} = \Delta\Delta S^{\text{translation}} + \Delta\Delta S^{\text{rotation}} + \Delta\Delta S^{\text{vibration}} - 4k_{\text{B}} \ln \phi \quad (1)$$

Here, $\Delta\Delta S^{\text{translation}}$, $\Delta\Delta S^{\text{rotation}}$, and $\Delta\Delta S^{\text{vibration}}$ represent the entropy penalty decrease from individual water molecules and $-4k_{\text{B}} \ln \phi$ denotes the entropy penalty decrease of water as a

collective network ($\Delta\Delta S^{\text{network}}$), with ϕ representing the ratio of water network sizes in ionic solutions and pure water (see **Supplementary Text** for derivation of eq. 1 and further details).

The total decrease of water entropy penalty from different ion pairs can be calculated using eq. 1 with values of individual contributions obtained from molecular dynamics simulation (Fig. 2D and fig. S9). Notably, the decrease of water network entropy penalty $\Delta\Delta S^{\text{network}}$ appears to be the predominant factor over contributions of rotational and translational entropy of individual water molecules, especially for LiBr and LiCl, the two potent protein denaturants (Fig. 2F). This key factor has been overlooked in several previous studies leading to considerable controversy regarding the effects of solutes on water dynamics and protein unfolding (*35*, *36*). Furthermore, the theoretically calculated $\Delta\Delta S^{\text{network}}$ and the experimentally observed ratio of denatured and native α-helix around 1650-1655 cm^{-1} from FTIR in LiBr and LiCl solutions showed a strong correlation with the Pearson correlation coefficient of 0.9058 (Fig. 2G). In contrast, contributions from rotational and translational entropy exhibited a weaker correlation (fig. S10), with minimal contributions to the total decrease of water entropy and misalignment with the denaturation capabilities of different salt solutions. The strong quantitative agreement between theoretical predictions and experimental results suggests the universal predictive capability of the water network model across various ion types and concentrations, particularly at conditions where water network entropy plays a dominant role. For salts and concentrations where $\Delta\Delta S^{\text{network}}$ is less than 10 J mol^{-1} K^{-1}, our model predicts no denaturation or indicates that water network entropy is not the primary driving force behind any observed denaturation, as exemplified by NaBr.

Finally, protein free energy landscapes at different LiBr concentrations were constructed using well-tempered metadynamics simulation (*37*) (See **Methods** for details), where a stable α-helix peptide of 20 amino acids was adopted as a model protein (Fig. 2H, and figs. S11 to S15).

201 The increase of ion concentrations shifts the free energy landscapes and lowers the energy barrier
202 for unfolding, which lends further confirmation of the universal denaturation capacity of LiBr.
203 Thus, solute-induced water network disruption potentiates the reduction of entropy penalty when
204 proteins sequester water molecules from bulk water network during unfolding. This facilitates
205 unfolding and potentiates large-scale protein conformational changes and denaturation.

206 **Keratin regeneration with closed-loop recycling and facile manufacturing**

207 In contrast with conventionally applied enthalpy-driven denaturants (e.g., urea, GdnHCl), the
208 entropy-driven denaturation mechanism can address limitations in protein regeneration, including
209 the waste and pollution from single-use organic chemicals and the complexity of fabrication.
210 Hereby, we developed an alternative protocol for keratin-rich waste regeneration with closed-loop
211 recycling of LiBr solution followed by facile manufacturing based on the entropy-driven
212 denaturation mechanism (Fig. 3A). Protein resources such as animal fragments or wool-based
213 textiles are denatured by an aqueous solution of 8 M LiBr, with heat applied to accelerate reaction
214 kinetics and prevent aggregation during extraction. A small amount of 1,4-dithiothreitol (DTT) is
215 added as a reducing agent to break down the dense disulfide matrix in keratin. After extraction,
216 the mixture is hot filtered, cooled down and separated into a subnatant of denatured keratin gel and
217 a supernatant of LiBr solution driven by spontaneous aggregation (fig. S16, A and B). Since the
218 LiBr does not induce denaturation via direct interactions, the resulting solution can be continuously
219 recycled in a closed loop, which not only eliminates pollution from waste organics but also
220 significantly reduces the consumption and cost of denaturants.

221 To test the cyclic stability of the closed-loop recycling protocol, we performed multiple
222 iterations of extraction using both α-keratin from wool and β-keratin from goose feathers. The
223 yield remains consistently around 40% after five cycles of extraction (Fig. 3B, and fig. S17), while

224 the first cycle exhibits a slightly lower yield possibly due to a small amount of keratin remaining
225 in the solution after separation. Unchanged composition of the recycled LiBr solution is further
226 confirmed with thermogravimetric analysis (TGA) and coupled Fourier transform infrared
227 spectroscopy (TG-FTIR) of the emerging gas (fig. S18).

228 Notably, in the absence of direct binding to denaturants, the spontaneous aggregation of
229 denatured keratin enables a simple separation of condensed gel from the solution, alleviating
230 difficulties with conventional organic reagents (fig. S16C), which usually involves dialysis and
231 lyophilization. Additionally, the separated keratin can undergo a fast phase transition from
232 denatured gel state to renatured solid state when transferring back into water (Fig. 3C, and movie
233 S1), while keratin extracted with organic denaturants remains non-processable until fully dialyzed
234 and lyophilized. The viscous property of the gel and the fast phase transition process enable a wide
235 array of manufacturing modalities including injection molding, membrane casting, dip coating,
236 fiber spinning, and 3D printing (Fig. 3D, and fig. S19) from a broad range of keratin sources (fig.
237 S20) without any additional usage of organic solvents.

238 **Mechanical tunability and shape-memory of regenerated keratin**

239 Keratins, particularly α-keratins, contain multiple cysteine residues, which form a dense network
240 of intermolecular disulfide bonds. After extraction, these disulfide bonds are reduced to thiol
241 groups, thereby endowing the regenerated keratin material with adjustable covalent crosslinking
242 through oxidation. For instance, low level of crosslinking allows the α-helices to rearrange more
243 freely under stress. As a result, reduced keratin preserves a high flexibility with a modulus of 124.3
244 ± 18.8 kPa and a fracture strain of 435 ± 61% (fig. S21, A to C). On the contrary, formation of
245 multiple disulfide bonds can significantly increase the elastic modulus of oxidized keratin by an
246 order of magnitude to 1.35 ± 0.11 MPa and decrease the fracture strain to 95 ± 9% (fig. S21, D to

247 F). Raman spectroscopy of keratin samples under 50% strain suggests that most secondary
248 structures remain unchanged within reduced keratin upon stretching, whereas a more discernible
249 loss of α-helix domains and an increase of β/random structures can be observed in oxidized keratin
250 (fig. S22). Differences between the two conditions reveal the effect of disulfide crosslinking on
251 the α-helix network of regenerated keratin, providing the material with tunable mechanical
252 properties from ductile to elastic (fig. S21, G to I).

253 Additionally, the capability of forming a homogenous object through the fast phase
254 transition in water and the preservation of the native α-helix structure provide a hydration-
255 responsive shape-memory property for the regenerated keratin. Prior studies of Miserez et al. (*38*)
256 and Cera et al. (*15*) revealed that uniaxial strain can induce reversible uncoiling of α-helix into
257 metastable β-like structures within anisotropic bio-based elastomer. Similarly, in the disulfide
258 crosslinked keratin material, the transition between coiled helix and uncoiled strands can also lead
259 to a shape-memory effect facilitated by formation and decay of hydrogen bonds (*39*). Dynamic
260 reformation of hydrogen bonds in a hydrated environment enables the reshaping of the object into
261 a temporary shape without breaking, which can then be locked temporarily through dehydration
262 due to the formation of intermolecular hydrogen bonds. Upon rehydration, the presence of free
263 water molecules can unlock the hydrogen bonds again and facilitate the recovery of native α-helix
264 structures and the permanent shape (Fig. 3E). Notably, this property has been observed exclusively
265 in natural keratin or keratin materials obtained using the LiBr regeneration strategy. In contrast,
266 traditional extraction methods generally result in dispersed powders or compromised secondary
267 structures (fig. S23, and table S1). The shape-memory capability of regenerated keratin material is
268 demonstrated both as a standalone object and as components of complex tensegrity structures (Fig.
269 3F, figs. S24 and S25, and movies S2-4).

Discussion

The effect of water networks on protein conformation and stability has long been a subject of extensive debate. Building on the foundational work dating back to the 19th century 'Hofmeister Series' and continuing to the present, we investigated the molecular mechanisms underlying hierarchical protein conformational changes in the presence of three monovalent salts—LiBr, LiCl, and NaBr. Notably, our ITC experiments revealed no direct interactions between proteins and ionic solutes despite the significant potency of LiBr as a universal denaturant. This result provides direct evidence of a new mechanism of denaturation that stands in contrast to the established mechanism of denaturation driven by direct binding of organic denaturants to proteins. Instead, it points to an alternative pathway driven by entropy rather than enthalpy.

Thermodynamic and spectroscopic analyses, in combination with atomistic molecular simulations, have shown that large-scale protein conformational changes and denaturation by LiBr and other ionic solutes are mediated by reduction of entropy penalty (Fig. 4). Localized strong solute-water interactions for LiBr, and, to a lesser extent, LiCl, disrupt the water network and reduce the entropy penalty that proteins incur when sequestering water molecules from bulk water phase during denaturation. In contrast, the integrity of water network is largely preserved in NaBr solution, thereby consistently retaining protein native structures across varying concentrations. This entropic mechanism of protein denaturation by salts like LiBr opens new opportunities in technological development of protein extraction from natural sources by alleviating the need in complex and environmentally hazardous steps of separation of organic denaturants from bulk proteins.

References

1. F. Hofmeister, Zur Lehre von der Wirkung der Salze. Archiv f. experiment. Pathol. u. Pharmakol 24, 247–260 (1888).
2. P. Jungwirth, P. S. Cremer, Beyond Hofmeister. Nature Chem 6, 261–263 (2014).
3. M. Feughelman, A. R. Haly, P. Mason, Contraction of Keratin Fibres in Aqueous Lithium Bromide. Nature 196, 957–958 (1962).
4. D. C. Carpenter, F. E. Lovelace, The Influence of Neutral Salts on the Optical Rotation of Gelatin. III. Effect of the Halides of Lithium, Sodium, Rubidium and Cesium1. J. Am. Chem. Soc. 57, 2337–2342 (1935).
5. L. Mandelkern, J. C. Halpin, A. F. Diorio, A. S. Posner, Dimensional Changes in Fibrous Macromolecules: The System α-Keratin-Lithium Bromide. J. Amer. Chem. Soc. 84, 1383–1391 (1962).
6. J. Bello, H. R. Bello, Evidence from model peptides relating to the denaturation of proteins by lithium salts. Nature 194, 681–682 (1962).
7. J. Bello, H. R. Bello, Interaction of Model Peptides with Water and Lithium Bromide. Nature 190, 440–441 (1961).
8. V. Balos, N. K. Kaliannan, H. Elgabarty, M. Wolf, T. D. Kühne, M. Sajadi, Time-resolved terahertz–Raman spectroscopy reveals that cations and anions distinctly modify intermolecular interactions of water. Nat. Chem. 14, 1031–1037 (2022).
9. V. Mazzini, V. S. J. Craig, Volcano Plots Emerge from a Sea of Nonaqueous Solvents: The Law of Matching Water Affinities Extends to All Solvents. ACS Cent Sci 4, 1056–1064 (2018).
10. M.-C. Bellissent-Funel, A. Hassanali, M. Havenith, R. Henchman, P. Pohl, F. Sterpone, D. van der Spoel, Y. Xu, A. E. Garcia, Water Determines the Structure and Dynamics of Proteins. Chem. Rev. 116, 7673–7697 (2016).
11. Y. Levy, J. N. Onuchic, Water mediation in protein folding and molecular recognition. Annu Rev Biophys Biomol Struct 35, 389–415 (2006).
12. K. A. Dill, T. M. Truskett, V. Vlachy, B. Hribar-Lee, Modeling water, the hydrophobic effect, and ion solvation. Annu Rev Biophys Biomol Struct 34, 173–199 (2005).
13. E. Shakhnovich, Protein Folding Thermodynamics and Dynamics: Where Physics, Chemistry and Biology Meet. Chem Rev 106, 1559–1588 (2006).
14. W. J. Xie, Y. Q. Gao, A Simple Theory for the Hofmeister Series. J Phys Chem Lett 4, 4247–4252 (2013).
15. L. Cera, G. M. Gonzalez, Q. Liu, S. Choi, C. O. Chantre, J. Lee, R. Gabardi, M. C. Choi, K. Shin, K. K. Parker, A bioinspired and hierarchically structured shape-memory material. Nat Mater 20, 242–249 (2021).
16. D. N. Rockwood, R. C. Preda, T. Yücel, X. Wang, M. L. Lovett, D. L. Kaplan, Materials fabrication from Bombyx mori silk fibroin. Nat Protoc 6, 1612–1631 (2011).
17. J. Sun, G. Monreal Santiago, F. Yan, W. Zhou, P. Rudolf, G. Portale, M. Kamperman, Bioinspired Processing of Keratin into Upcycled Fibers through pH-Induced Coacervation. ACS Sustainable Chem. Eng. 11, 1985–1994 (2023).
18. N. Senthilkumar, S. Chowdhury, P. Sanpui, Extraction of keratin from keratinous wastes: current status and future directions. J Mater Cycles Waste Manag 25, 1–16 (2023).
19. K. Niinimäki, G. Peters, H. Dahlbo, P. Perry, T. Rissanen, A. Gwilt, The environmental price of fast fashion. Nat Rev Earth Environ 1, 189–200 (2020).
20. W. Fang, R. Fan, A. S. Aranko, M. Hummel, H. Sixta, Upcycling of Keratin Wastes in Sustainable Textile Fiber Applications. ACS Sustainable Chem. Eng. 11, 14807–14815 (2023).
21. S. Zhu, Q. Zhou, J. Yi, Y. Xu, C. Fan, C. Lin, J. Wu, Y. Lin, Using Wool Keratin as a Structural Biomaterial and Natural Mediator to Fabricate Biocompatible and Robust Bioelectronic Platforms. Adv Sci (Weinh) 10, e2207400 (2023).

22. C. J. Dalton, C. A. Lemmon, Fibronectin: Molecular Structure, Fibrillar Structure and Mechanochemical Signaling. Cells 10, 2443 (2021).
23. A. W. Feinberg, K. K. Parker, Surface-Initiated Assembly of Protein Nanofabrics. Nano Lett. 10, 2184–2191 (2010).
24. S. Ahn, L. F. Deravi, S.-J. Park, B. E. Dabiri, J.-S. Kim, K. K. Parker, K. Shin, Self-Organizing Large-Scale Extracellular-Matrix Protein Networks. Advanced Materials 27, 2838–2845 (2015).
25. S. Ahn, K. Y. Lee, K. K. Parker, K. Shin, Formation of Multi-Component Extracellular Matrix Protein Fibers. Sci Rep 8, 1913 (2018).
26. L. F. Deravi, T. Su, J. A. Paten, J. W. Ruberti, K. Bertoldi, K. K. Parker, Differential Contributions of Conformation Extension and Domain Unfolding to Properties of Fibronectin Nanotextiles. Nano Lett. 12, 5587–5592 (2012).
27. P. L. Privalov, Stability of proteins: small globular proteins. Adv Protein Chem 33, 167–241 (1979).
28. E. P. O'Brien, R. I. Dima, B. Brooks, D. Thirumalai, Interactions between hydrophobic and ionic solutes in aqueous guanidinium chloride and urea solutions: Lessons for protein denaturation mechanism. Journal of the American Chemical Society 129, 7346–7353 (2007).
29. M. C. Stumpe, H. Grubmüller, Interaction of urea with amino acids: implications for urea-induced protein denaturation. J Am Chem Soc 129, 16126–16131 (2007).
30. N. T. Skipper, G. W. Neilson, X-ray and neutron diffraction studies on concentrated aqueous solutions of sodium nitrate and silver nitrate. J. Phys.: Condens. Matter 1, 4141 (1989).
31. K. J. Tielrooij, N. Garcia-Araez, M. Bonn, H. J. Bakker, Cooperativity in ion hydration. Science 328, 1006–1009 (2010).
32. W. L. Jorgensen, J. Chandrasekhar, J. D. Madura, R. W. Impey, M. L. Klein, Comparison of simple potential functions for simulating liquid water. The Journal of Chemical Physics 79, 926–935 (1983).
33. S.-T. Lin, P. K. Maiti, W. A. Goddard, Two-phase thermodynamic model for efficient and accurate absolute entropy of water from molecular dynamics simulations. J Phys Chem B 114, 8191–8198 (2010).
34. S. A. Roget, T. R. Heck, K. A. Carter-Fenk, M. D. Fayer, Ion/Water Network Structural Dynamics in Highly Concentrated Lithium Chloride and Lithium Bromide Solutions Probed with Ultrafast Infrared Spectroscopy. J Phys Chem B 127, 4532–4543 (2023).
35. Y. Harano, M. Kinoshita, Translational-Entropy Gain of Solvent upon Protein Folding. Biophysical Journal 89, 2701–2710 (2005).
36. H. I. Okur, J. Hladílková, K. B. Rembert, Y. Cho, J. Heyda, J. Dzubiella, P. S. Cremer, P. Jungwirth, Beyond the Hofmeister Series: Ion-Specific Effects on Proteins and Their Biological Functions. J. Phys. Chem. B 121, 1997–2014 (2017).
37. G. Fiorin, M. L. Klein, J. Hénin, Using collective variables to drive molecular dynamics simulations. Molecular Physics 111, 3345–3362 (2013).
38. A. Miserez, S. S. Wasko, C. F. Carpenter, J. H. Waite, Non-entropic and reversible long-range deformation of an encapsulating bioelastomer. Nat Mater 8, 910–916 (2009).
39. X. Xiao, J. Hu, Animal Hairs as Water-stimulated Shape Memory Materials: Mechanism and Structural Networks in Molecular Assemblies. *Sci Rep* **6**, 26393 (2016).
40. J. C. Phillips, D. J. Hardy, J. D. C. Maia, J. E. Stone, J. V. Ribeiro, R. C. Bernardi, R. Buch, G. Fiorin, J. Hénin, W. Jiang, R. McGreevy, M. C. R. Melo, B. K. Radak, R. D. Skeel, A. Singharoy, Y. Wang, B. Roux, A. Aksimentiev, Z. Luthey-Schulten, L. V. Kalé, K. Schulten, C. Chipot, E. Tajkhorshid, Scalable molecular dynamics on CPU and GPU architectures with NAMD. *J Chem Phys* **153**, 044130 (2020).
41. W. Humphrey, A. Dalke, K. Schulten, VMD: visual molecular dynamics. *J Mol Graph* **14**, 33–38, 27–28 (1996).
42. J. A. Maier, C. Martinez, K. Kasavajhala, L. Wickstrom, K. E. Hauser, C. Simmerling, ff14SB: Improving the accuracy of protein side chain and backbone parameters from ff99SB. *J Chem Theory Comput* **11**, 3696–3713 (2015).

43. D. J. Price, C. L. Brooks III, A modified TIP3P water potential for simulation with Ewald summation. *The Journal of Chemical Physics* **121**, 10096–10103 (2004).
44. P. Li, L. F. Song, K. M. Merz, Parameterization of highly charged metal ions using the 12-6-4 LJ-type nonbonded model in explicit water. *J Phys Chem B* **119**, 883–895 (2015).
45. D. A. Case, T. E. Cheatham, T. Darden, H. Gohlke, R. Luo, K. M. Merz, A. Onufriev, C. Simmerling, B. Wang, R. J. Woods, The Amber biomolecular simulation programs. *J Comput Chem* **26**, 1668–1688 (2005).
46. S.-T. Lin, M. Blanco, W. A. Goddard III, The two-phase model for calculating thermodynamic properties of liquids from molecular dynamics: Validation for the phase diagram of Lennard-Jones fluids. *The Journal of Chemical Physics* **119**, 11792–11805 (2003).
47. atlas-nano/2PT, ATLAS Materials Physics Lab (2024); https://github.com/atlas-nano/2PT.
48. S. Marqusee, V. H. Robbins, R. L. Baldwin, Unusually stable helix formation in short alanine-based peptides. *Proc Natl Acad Sci U S A* **86**, 5286–5290 (1989).
49. M. Mirdita, K. Schütze, Y. Moriwaki, L. Heo, S. Ovchinnikov, M. Steinegger, ColabFold: making protein folding accessible to all. *Nat Methods* **19**, 679–682 (2022).
50. G. A. Tribello, M. Bonomi, D. Branduardi, C. Camilloni, G. Bussi, PLUMED 2: New feathers for an old bird. *Computer Physics Communications* **185**, 604–613 (2014).
51. Y. Ozaki, Y. Takagi, H. Mori, M. Hara, Porous hydrogel of wool keratin prepared by a novel method: An extraction with guanidine/2-mercaptoethanol solution followed by a dialysis. *Materials Science and Engineering: C* **42**, 146–154 (2014).
52. S. Deb-Choudhury, J. E. Plowman, D. P. Harland, Isolation and Analysis of Keratins and Keratin-Associated Proteins from Hair and Wool. *Methods Enzymol* **568**, 279–301 (2016).
53. K. Kadirvelu, N. N. Fathima, Self-assembly of keratin peptides: Its implication on the performance of electrospun PVA nanofibers. *Sci Rep* **6**, 36558 (2016).
54. K. R. Ramya, R. Thangam, B. Madhan, Comparative analysis of the chemical treatments used in keratin extraction from red sheep's hair and the cell viability evaluations of this keratin for tissue engineering applications. *Process Biochemistry* **90**, 223–232 (2020).
55. C. Earland, C. S. Knight, Studies on the structure of keratin. I. The analysis of fractions isolated from wool oxidized with peracetic acid. *Biochim Biophys Acta* **17**, 457–461 (1955).
56. J. M. Cardamone, Investigating the microstructure of keratin extracted from wool: Peptide sequence (MALDI-TOF/TOF) and protein conformation (FTIR). *Journal of Molecular Structure* **969**, 97–105 (2010).
57. L. Zhang, P. Zhu, S. Ying Sui, C. Hong Dong, J. Tao Xu, Study on the Extraction and Properties of Human Hair Proteins. *Integrated Ferroelectrics* **160**, 169–174 (2015).
58. A. J. Poole, J. S. Church, The effects of physical and chemical treatments on Na2S produced feather keratin films. *International Journal of Biological Macromolecules* **73**, 99–108 (2015).
59. A. P. Bhat, C. R. Holkar, A. J. Jadhav, D. V. Pinjari, Acoustic and hydrodynamic cavitation assisted hydrolysis and valorisation of waste human hair for the enrichment of amino acids. *Ultrasonics Sonochemistry* **71**, 105368 (2021).
60. H. Xie, S. Li, S. Zhang, Ionic liquids as novel solvents for the dissolution and blending of wool keratin fibers. *Green Chem.* **7**, 606–608 (2005).
61. K. S. Lovejoy, A. J. Lou, L. E. Davis, T. C. Sanchez, S. Iyer, C. A. Corley, J. S. Wilkes, R. K. Feller, D. T. Fox, A. T. Koppisch, R. E. Del Sesto, Single-Pot Extraction-Analysis of Dyed Wool Fibers with Ionic Liquids. *Anal. Chem.* **84**, 9169–9175 (2012).
62. Y. Ji, J. Chen, J. Lv, Z. Li, L. Xing, S. Ding, Extraction of keratin with ionic liquids from poultry feather. *Separation and Purification Technology* **132**, 577–583 (2014).
63. C. Apostolidou, Regenerated Hoof Keratin from 1-Ethyl-3-Methylimidazolium Acetate and Insights into Disulfide-Ionic Liquid Interactions from MD Simulation. *ChemistryOpen* **9**, 695–702 (2020).
64. M. Zoccola, A. Aluigi, A. Patrucco, C. Vineis, F. Forlini, P. Locatelli, M. C. Sacchi, C. Tonin, Microwave-assisted chemical-free hydrolysis of wool keratin. *Textile Research Journal* **82**, 2006–2018 (2012).

65. F. Bertini, M. Canetti, A. Patrucco, M. Zoccola, Wool keratin-polypropylene composites: Properties and thermal degradation. *Polymer Degradation and Stability* **98**, 980–987 (2013).
66. J. Chen, S. Ding, Y. Ji, J. Ding, X. Yang, M. Zou, Z. Li, Microwave-enhanced hydrolysis of poultry feather to produce amino acid. *Chemical Engineering and Processing: Process Intensification* **87**, 104–109 (2015).
67. C. Tonin, M. Zoccola, A. Aluigi, A. Varesano, A. Montarsolo, C. Vineis, F. Zimbardi, Study on the Conversion of Wool Keratin by Steam Explosion. *Biomacromolecules* **7**, 3499–3504 (2006).
68. Y. Zhang, W. Zhao, R. Yang, Steam Flash Explosion Assisted Dissolution of Keratin from Feathers. *ACS Sustainable Chem. Eng.* **3**, 2036–2042 (2015).
69. J. Yin, S. Rastogi, A. E. Terry, C. Popescu, Self-organization of Oligopeptides Obtained on Dissolution of Feather Keratins in Superheated Water. *Biomacromolecules* **8**, 800–806 (2007).
70. K. Tasaki, A novel thermal hydrolysis process for extraction of keratin from hog hair for commercial applications. *Waste Management* **104**, 33–41 (2020).
71. N. Zhang, Q. Wang, J. Yuan, L. Cui, P. Wang, Y. Yu, X. Fan, Highly efficient and eco-friendly wool degradation by L-cysteine-assisted esperase. *Journal of Cleaner Production* **192**, 433–442 (2018).
72. Z. Peng, X. Mao, J. Zhang, G. Du, J. Chen, Efective biodegradation of chicken feather waste by co-cultivation of keratinase producing strains. *Microbial Cell Factories*, doi: 10.1186/s12934-019-1134-9 (2019).
73. C. Su, J.-S. Gong, J.-P. Ye, J.-M. He, R.-Y. Li, M. Jiang, Y. Geng, Y. Zhang, J.-H. Chen, Z.-H. Xu, J.-S. Shi, Enzymatic Extraction of Bioactive and Self-Assembling Wool Keratin for Biomedical Applications. *Macromol Biosci* **20**, e2000073 (2020).
74. Y. Lai, X. Wu, X. zheng, W. Li, L. Wang, Insights into the keratin efficient degradation mechanism mediated by Bacillus sp. CN2 based on integrating functional degradomics. *Biotechnol Biofuels Bioprod* **16**, 59 (2023).
75. C. H. Zeng, Q. Lu, Study on the Recovery of Waste Wool by Combining Reduction and Metallic Salt Methods. *Advanced Materials Research* **881–883**, 551–555 (2014).
76. Y. Wang, T. Zhang, F. Wang, L. Zhang, Y. Peng, M. Zhang, F. Ran, Efficient Extraction of Wool Keratin Governed by Simultaneous Cation and Anion Effects: From Secondary Structure Studies to High α-Helix Keratin Content. *ACS Sustainable Chem. Eng.* **12**, 6003–6012 (2024).

Data availability All the source data can be readily accessed via https://doi.org/10.7910/DVN/U6HAQS

Code availability All the customized codes used for data analysis are available at https://github.com/junlang-liu/Entropy_code

Acknowledgements We thank M. Rosnach for photography and illustrations, S. Mondal for suggestions on molecular simulations, K. Park, E. Serebryany and A. Bitran for discussions on water structure and protein denaturation mechanisms, H. Chang and J. F. Zimmerman for discussions on material properties. K. Shani and Y. Jang for discussions on biological properties and tissue engineering potential of keratin. This work was sponsored by National Institutes of Health (R35GM139571 and R01EY030444 to E.I.S), the John A. Paulson School of Engineering and Applied Sciences at Harvard University (K.K.P.), the National Science Foundation through the Harvard University Materials Research Science and Engineering Center (DMR-2011754 to K.K.P.), the Health@InnoHK program of the Innovation and Technology Commission of the Hong Kong SAR Government, and the Medical & Health Informatics Laboratories at NTT Research, Inc. This work was performed in part at the Harvard University Center for Nanoscale Systems (CNS), a member of the National Nanotechnology Coordinated Infrastructure Network (NNCI), which is supported by the National Science Foundation under NSF award no. ECCS-2025158. The content is solely the responsibility of the authors and does not necessarily represent the official views of NTT Research, Inc.

Author contributions Y.W., J.L., K.K.P., and E.I.S. designed and developed the project. Y.W. and J.L. performed turbidity measurements, tryptophan fluorescence, and FTIR. Y.W., J.L., and D.W. performed ITC experiments. Y.W., J.L., and S.C. performed Raman experiments. J.L. did *E. coli* cell culture, DHFR protein purification and quality control. J.L. conceived the entropy-driven model and developed the analytical model. J.L. conducted all the simulations and related data analysis. Y.W. performed TG-FTIR, polarized Raman, DLS, and TGA measurements. Y.W. performed keratin extraction, mechanical tests, and demonstrations. Y.W. and M.M.P. fabricated keratin fibers and performed SEM imaging. Y.W. and R.I. did SDS-PAGE. Y.W. and J.L. prepared the initial manuscript. Y.W., J.L., K.K.P., and E.I.S. revised the manuscript, with contributions from all the other authors. K.K.P. and E.I.S. supervised the research.

Competing interests A US patent application on the methods for extraction and regeneration of protein wastes has been filed by Harvard University (inventors: Y.W., J.L., K.K.P., and E.I.S.).

Supplementary materials
Materials and Methods
Supplementary Text
Figs. S1 to S25
Tables S1 and S2

Correspondence and requests for materials should be addressed to Eugene I. Shakhnovich or Kevin Kit Parker

Figures

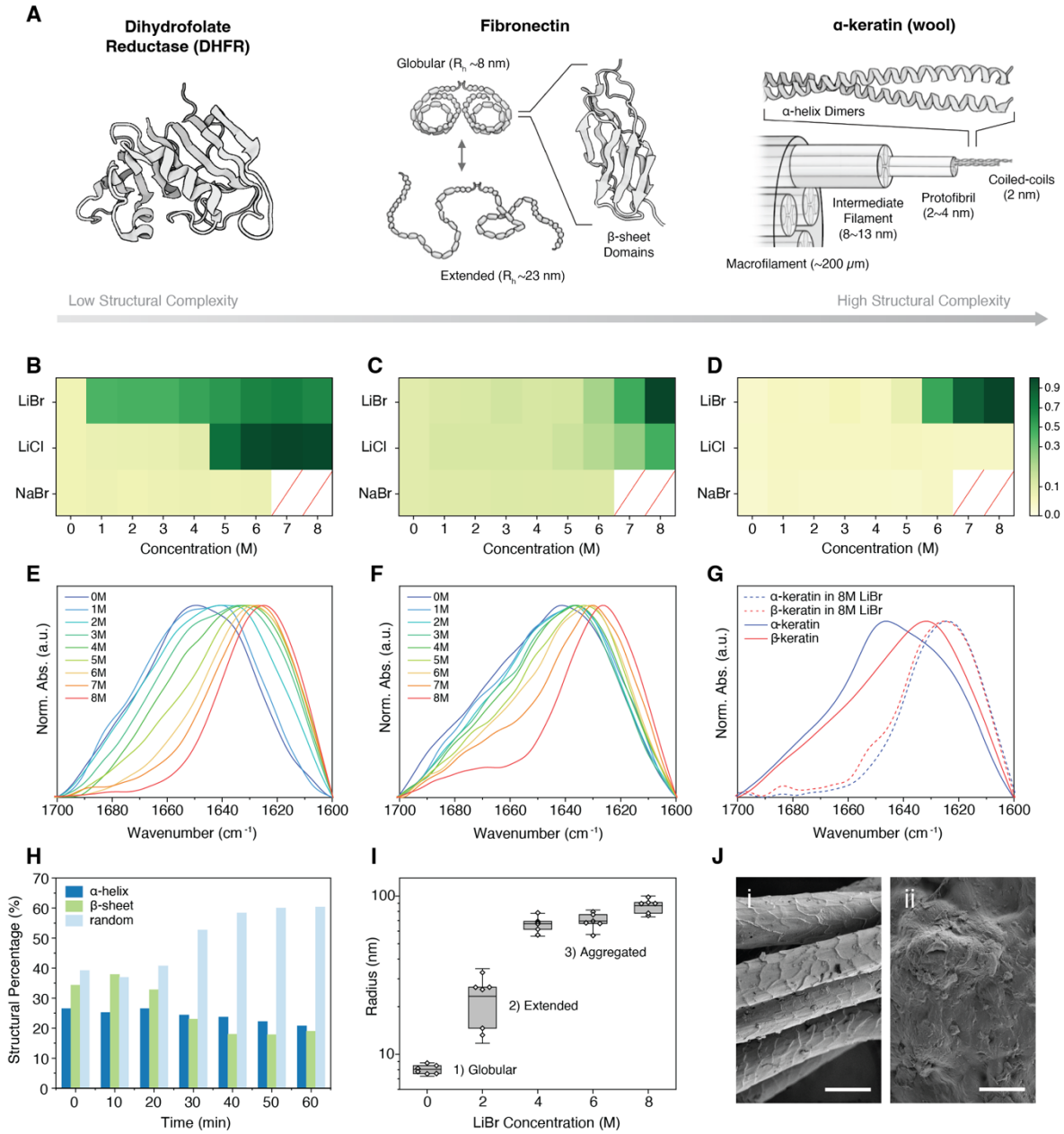

Fig. 1. Concentrated LiBr solutions induce universal protein conformational change and cause denaturation. (**A**), Schematics of DHFR, fibronectin, and α-keratin (wool), representing three levels of structural complexity. (**B-D**) Turbidity assay of three respective proteins measured by OD_{405}, suggesting different denaturation capabilities of LiBr, LiCl, and NaBr. Data are normalized by the highest OD_{405} values of respective proteins and presented as mean (n = 4). (**E-G**), FTIR of the amide I band indicate a gradual loss of secondary structure upon increasing of LiBr concentration. (**H**), Percentage change of the secondary structure in DHFR in 2 M LiBr, deconvoluted from the amide I band of Raman spectra. (**I**), DLS measurement of the hydrodynamic radius of fibronectin with increasing LiBr concentration, indicating an extension of quaternary structure followed by aggregation. Data are presented as mean ± 1.5 s.d. (n = 6). (**J**), SEM image of wool prior (i) and after (ii) denaturation with 8 M LiBr. Scale bars, 50 μm.

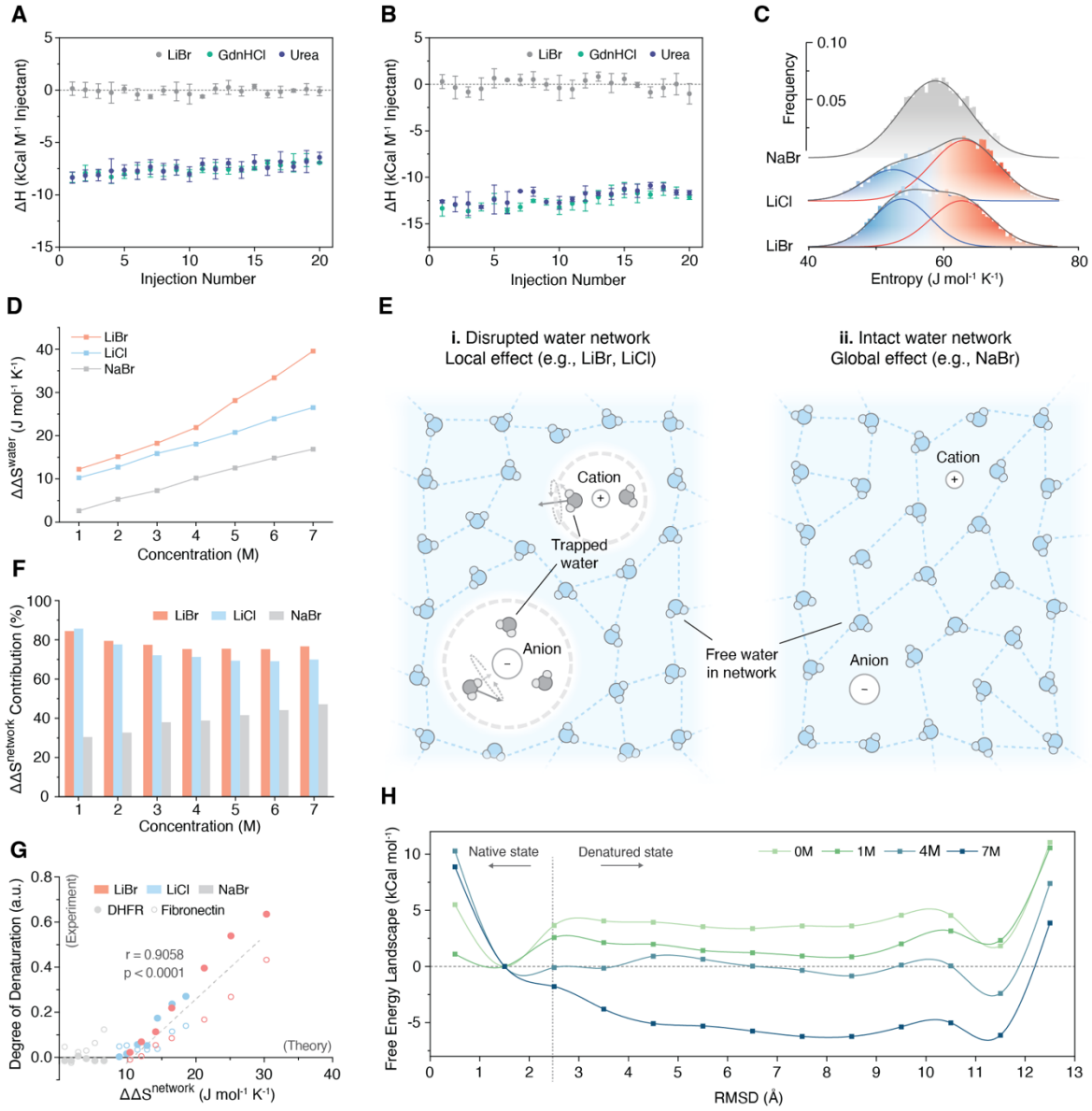

Fig. 2. Protein conformational changes come from indirect solute effects manifested as water network entropy. (**A** and **B**), Reaction enthalpy of interactions between proteins (**A,** DHFR, **B,** fibronectin) and denaturants (LiBr, urea, and GdnHCl) as measured by isothermal titration calorimetry. Data are presented as mean ± s.d. (n = 3). (**C**), Distributions of molecular entropy of water molecules in 7 M LiBr, LiCl, and NaBr from MD simulations. (**D**), Total water entropy penalty decrease in different concentrations of LiBr, LiCl, and NaBr solutions. Data are obtained from MD simulations and calculated via the analytical model (Eq. 1). Data are presented as mean ± s.d. (n = 3), however, the error bars are smaller than the data point size. (**E**), Schematics of different ion effects on water structures. For LiBr and LiCl, high charge density of Li^+ ion results in localized (trapped) water molecules and disrupted water network (**i**), while NaBr induces a more global effect without breaking water network (**ii**). (**F**), Contribution of water network entropy penalty decrease to the total water entropy penalty decrease presented in (**D**). (**G**), Strong correlation between the theoretical value of water network entropy penalty decrease and the protein denaturation ratio observed from FTIR experiments in LiBr and LiCl solutions. Pearson correlation coefficient calculated with a 95% confidence interval for a two-tailed test. Dashed line represents the best fit. (**H**), Free energy landscape of an α-helix peptide (20 amino acids) in pure water and 1, 4, 7 M LiBr from MD simulations.

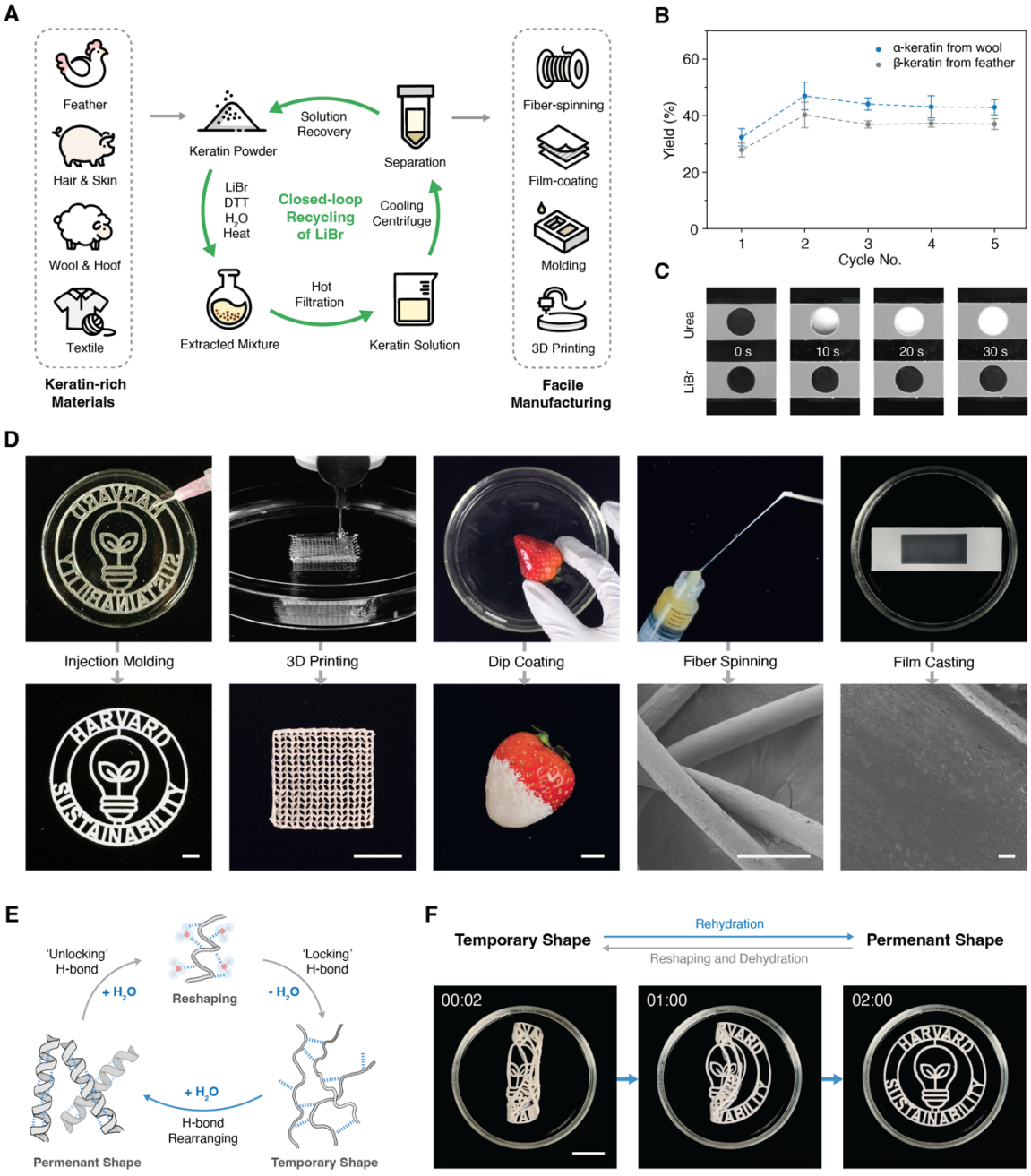

Fig. 3. Keratin regeneration with closed-loop recycling and facile manufacturing. (**A**), Schematic showing the regeneration protocol of keratin materials with closed-loop recycling of LiBr solution. (**B**), Extraction yield of α-keratin from wool and β-keratin from goose down. Data are presented as mean ± s.d. (n = 7 for α-keratin, n = 3 for β-keratin). (**C**), Immersing extracted keratin in transparent well spacers in water. Keratin gel from LiBr extraction quickly turns into a white solid phase, while keratin solution extracted with urea remains soluble. (**D**), Facile manufacturing strategies including injection molding, 3D printing, dip coating, fiber spinning, and membrane casting. Scale bars, 1 cm for optical images, 200 μm for SEM images. (**E**), Schematic of the shape memory effect triggered by hydration signal. (**F**), Demonstration of shape memory effect by placing a dehydrated keratin sample in water. Scale bar: 3 cm.

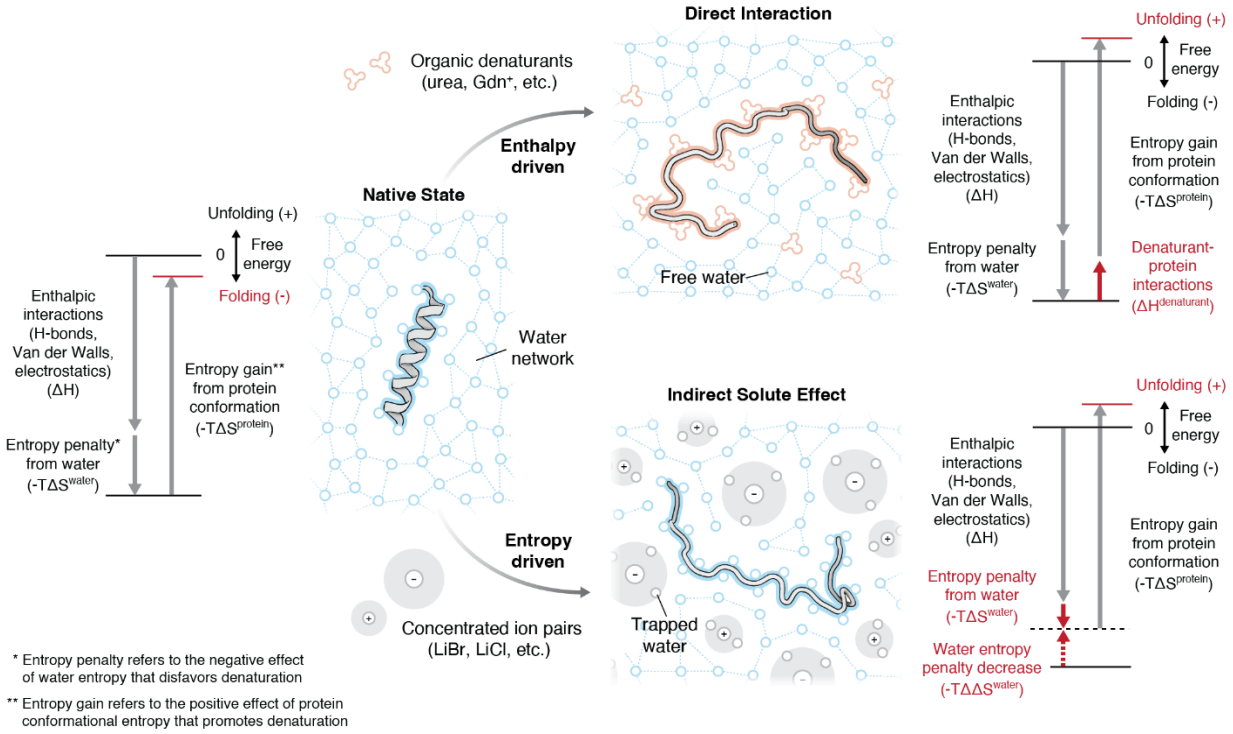

Fig. 4. Mechanistic comparison of enthalpy-driven denaturation and entropy-driven denaturation. In native state, proteins adopt a folded conformation driven by the combined effect of enthalpy and entropy. Traditional organics denaturants, such as urea and Gdn^+, interact directly with proteins, introducing additional enthalpic contributions that shift the equilibrium toward the unfolded state. In contrast, concentrated ion pairs, such as LiBr, disrupt the water network, decreasing the entropy penalty associated with protein-water interactions, and thereby achieve protein denaturation indirectly through an entropy-driven mechanism.